Bridging Tribology and Microrheology of Thin Films

CHRISTIAN CLASEN[*], H. PIROUZ KAVEHPOUR[‡], GARETH H. MCKINLEY[†],

[*] Laboratory of Applied Rheology and Polymer Processing, Department of Chemical Engineering, Katholieke Universiteit Leuven, Leuven, Belgium
[‡] Complex Fluids & Interfacial Physics Laboratory, Department of Mechanical & Aerospace Engineering, University of California, Los Angeles, CA, USA
[†] Hatsopoulos Microfluids Laboratory, Department of Mechanical Engineering, Massachusetts Institute of Technology, Cambridge, MA, USA

Abstract

An enhanced version of the flexure-based microgap rheometer (FMR) is described which enables rheological measurements in steady state shearing flows of bulk fluid samples of PDMS with an absolute gap separation between the shearing surfaces of 100 nm – 100 µm. Alignment of the shearing surfaces to a parallelism better then 10^{-7} rad allows us to reliably measure shear stresses at shear rates up to 10^4 s^{-1}. At low rates and for shearing gaps < 5 µm the stress response is dominated by sliding friction between the surfaces that is independent of the viscosity of the fluid and only determined by the residual particulate phase (dust particles) in the fluid. This behaviour is similar to the boundary lubrication regime in tribology. The absolute gap control of the FMR allows us to systematically investigate the flow behaviour at low degrees of confinement that cannot be accessed with conventional (controlled normal load) tribological test protocols.

Keywords: microrheology, thin film rheology, tribology, boundary lubrication, sliding plate rheometer, micro gap, FMR

Introduction

Tribology and lubrication have traditionally been considered to be distinct subjects set apart from classical bulk rheology and the rapidly developing area of microrheological investigation. The principal reason for this separation is that although fluid properties are key to the flow and friction phenomena observed in each field, the experimental approach and the resulting terminology differ substantially and prohibit a direct translation of the results. In particular the lack of well-defined viscometric kinematics for tribological experiments and the

difficulties in achieving sufficiently-precise fixture alignment in regular rheometry have inhibited the unification of results from these fields. This is particularly disappointing, because measurements of the steady shear rheology of thin films yields information that localized microrheological techniques cannot provide. In contrast to particulate probe methods [1,2,3,4,5], diffusive wave spectroscopy [6,7] or AFM techniques [8,9] that are often collectively referred to as 'microrheology' [10], material testing of a fluid film with a defined micro- to nanometer thickness allows one to access the full nonlinear rheological property response of a bulk sample and to identify the effects of confinement on the fluid rheology as a single characteristic dimension is progressively decreased until the 'tribological' interaction of the bounding surfaces dominate the response of the system.

From an experimental point of view, tribology and bulk shear rheology are very similar. Both techniques utilize the same basic measurement principles; i.e. they determine a force or torque that is transferred through the fluid from one shearing surface to another as a function of a velocity or angular velocity. However, traditionally tribology describes the transmission of a force between two shearing interfaces via the direct interaction of these surfaces (established by a normal load that forces the asperities on the surfaces into contact), moderated by a lubricating liquid. Shear rheology of bulk fluid samples, on the other hand, describes the transmission of forces between two shearing interfaces solely via the fluid, carefully avoiding the influence of any direct interaction of the surfaces or any kinematic discontinuities at the interfaces such as slip. However, as soon as the gap distance between the two shearing surfaces reaches the dimensions of the microstructure of a complex liquid, the distinction between tribology and shear rheology becomes fuzzy. As pointed out by McKenna[11], it becomes increasingly important to separate the bulk rheological response of a sample from effects due to the confining surfaces Although we are still performing a rheological experiment - with well-defined dimensions for the shearing surfaces and a well-controlled gap between them - the momentum transfer between the surfaces can be dominated by the confined microstructure of the liquid for small gaps. This also can happen for apparently simple fluids, since airborne dust particles and other contaminants lead to a direct interaction of the surfaces at gaps below approximately 3 µm as described by Granick and co-workers [12]. For a wide range of complex fluids, ranging from colloidal-sized suspensions to immiscible blends and other multicomponent systems, we expect to observe a complex material response that can be interpreted from a tribological as well as rheological point of view; thus bridging the gap between these two important but distinct experimental techniques. However, there are

few techniques that enable experimental exploration into this mesoscopic region characterized by gap separations of order O(1 μm).

Shear rheological experiments that approach this small gap separation are carried out for three principal purposes. Firstly, if the available sample volume itself is small, a bulk rheological experiment can only be carried out for a given shearing surface area if the gap separation is small. These investigations generally neglect the effect of geometric confinement and mostly examine simple fluids. Moon et al. [13] have recently introduced the multi-sample micro-slit rheometer (MMR) that determines the viscosity of pressure-driven polymer melts and other viscous liquids flowing through a 132 μm high channel by optically monitoring the propagation of the flow front. Similar approaches that apply a controlled pressure difference to a (micro)slit channel have been followed by Aramphongphun and Castro [14] and by Son [15]. Xie et al. [16] used the pressure drop observed for the radial flow between two self-aligning parallel disks in order to determine the shear viscosity down to gap separations of 50 μm. The emerging area of microfluidic device fabrication has also yielded approaches to determine the viscosity of liquids flowing in micrometer sized channels. The simplest approaches require a reference fluid against which the test sample is compared; as for example Han et al. [17] who built a miniaturized version of a classical capillary viscometer; Srivastava et al. [18] who use the capillary pressure of the leading meniscus in a micro slit channel as the driving force and determine the propagation speed of the liquid front; and Guillot et al. [19] and Nguyen et al. [20] who use an optical investigation of interface profiles of two fluids in laminar parallel flow within a microchannel. Degre et al. determine the velocity profile and steady flow curve using a pressure driven flow in a microfluidic channel coupled with PIV techniques [21]. There have also been approaches to incorporate pressure sensors directly into the channel for an *in situ* determination of the pressure drop as demonstrated by Chevalier et al. [22] and recently by Pipe et al. [23].

Secondly, if the gap distance is small, it is possible to reach much higher shear rates for a given shearing velocity, thus meeting industrial needs in the painting, coating or paper industries to probe the response of a fluid at high deformation rates. Experimental approaches include high pressure capillary or microchannel rheometers [24,25,26], rotary parallel plate rheometers operating at micrometer gaps [23,27,28,29,30,31,32], small gap Searl type geometries, operating at a constant gaps down to 1 μm [33] or small angled cup/bob devices that allow systematic variation of a small, relative gap [34]. These techniques aim to investigate

rheological properties of the bulk sample at high shear rates, therefore often deliberately neglecting the possible effects of geometric confinement that might become important at small gaps. However, when the characteristic length scale of the flow is reduced to microscopic scales, boundary effects such as wall-slip [35,36] or cohesive [37] and adhesive failure [38] occur on the same scale as the overall deformation of the bulk sample and their impact on the measured rheological properties can no longer be neglected. For homogeneous samples, slip, if present, occurs over length scales 0–50 nm [39] and is therefore usually negligible. However, for heterogeneous liquids with characteristic microstructural length scales of O(1-10 μm), slip effects caused by depletion or adhesion layers at the walls are readily observed [21,40]. These effects are localized at the boundary between the bulk sample and the shearing surface but their impact on the bulk flow cannot be neglected.

Shear rheological experiments with small gaps can also be used to investigate the influence of the fluid microstructure on the bulk material response under conditions in which the microstructural components themselves are confined by the shearing surfaces. For many complex liquids such as foods and other consumer products, these effects can become important even when the shearing gap is as large as O(10 μm). Many early investigations of the effect of geometric confinement were actually performed by *increasing* the dimensions of the microstructural elements rather than decreasing the confining gap; it is then possible for two phase polymer blends and emulsions to be investigated under confined conditions in conventional rheometric geometries with gaps between shearing surfaces that are greater than 50 μm. Examples include visual observation of the confined motion of single droplets in cylindrical tubes [41,42,43,44,45], Couette cells [46] or parallel plates [47]. Pronounced effects of geometrical confinement can be observed on features such as the critical capillary number for droplet breakup [48] and the corresponding breakup mechanism [49,50,51]. For suspensions, such ‘scale-up’ experiments make it possible to observe the effect of macroscopic interfaces on the volume fractions at which phase transitions occur [52,53,54,55]. However, little information is available on the relation of the state of stress to the observed deformations or on the morphology development during shearing flows in thin fluid films (with thicknesses on the order of micrometers). In order to investigate these phenomena and the more general effects of geometric confinement on the flow of complex media, techniques are necessary that probe the effective rheological properties of these samples on a microscopic length scale.

However, most of the rheological techniques that are capable of quantitative investigations at micrometer dimensions – and that are therefore generally labelled with the term 'microrheometry' – typically only study the local response of a sample. The field of microrheometry includes passive techniques that rely either on direct microscopic observations of Brownian motion [56] as well as single and multiple light scattering techniques, e.g. diffusing wave spectroscopy [7,57]. Actively-driven techniques that directly measure the forces on microscopic beads have also been developed using optical traps [58,59] and magnetic tweezers [60,61]. For recent reviews on the applications and evaluations of these microrheometrical techniques see [10,62,63,64].

There are also techniques that allow probing of molecular thin films of a sample via atomic force microscope (AFM) techniques [9,65,66] nanoindentation [67] or variants of the Surface Force Apparatus (SFA) [68,69,70]. For the smooth surfaces and thin gaps attained in the SFA, very pronounced and unexpected effects of confinement may arise. These phenomena have been referred to collectively as "nanorheology" and have been studied extensively by Granick and coworkers [70,71]. While these investigations actually present an example of confining a bulk sample of a complex fluid, the dimensions of the gap in the SFA are constrained to nanometer dimensions, and the available surfaces are typically restricted to opposed cylinders of cleaved mica.

The intermediate micro to 'meso-scale' range (roughly spanning gap separations of 0.1 μm – 10 μm) cannot be readily probed with either conventional bulk rheometry or nanoscale measurements of the apparent viscosity or surface friction. When the fluid film thickness is increased from a monolayer to a thin but continuous film, both bulk and 'nanorheological' contributions become important. Moreover, none of the techniques reviewed above allows probing of the non-linear rheological response of thin films to the large deformation amplitudes and rates that occur in most real flows of complex fluids. It is only recently that techniques have been developed to probe the true viscometric material functions of a bulk sample of a complex fluid under homogeneous deformation conditions on the meso to micro-scales.

Granick and co-workers developed a microgap rheometer that is capable of operating at 'mesoscale' gaps of 3 – 500 μm [12,70] and which can perform small amplitude oscillatory shear experiments [72]. This device is limited to the linear deformation regime due to the construction of the translator setup. Several designs of piezoelastic vibrators allow probing the linear

viscoelastic regime of liquids at gap settings between 10 and 100 µm [73,74,75] and this has resulted recently in a controversial discussion on the limits of these techniques [11,76]. Meeten [77] performed squeeze flow experiments using a spherical/flat surface combination on samples with thicknesses that cover a range from 100-1 µm. Mackay and coworkers showed that it is possible (with a very well-aligned rotational rheometer and specially-machined parallel plates) to perform reliable steady shear experiments down to gaps of 10 µm [78]. Stokes and co-workers recently presented a study [28] in which they evaluated the capability of commercially available rotary rheometers for accessing shearing gaps below 100 µm with parallel plates of 60 mm diameter. A careful correction of results obtained with a plate-plate geometry, taking into account fluid inertia [79] and gap errors due to non-parallelism [27,30] allowed them to perform steady shear flow experiments for gaps down to 20 µm. Clasen et al. [40,62] introduced the flexure-based microgap rheometer (*FMR*), a sliding plate configuration that utilizes white light interferometry (similar to the setup of Granick [12,72]) to set and maintain absolute gaps in the range of 1 - 100 µm. The compound-flexure-based translation mechanism of the FMR is optimized for applying non-linear deformations and performing steady shear flow experiments, but is less well suited to oscillatory measurements because of the large inertial mass.

So far only the work of Davies and Stokes [28,80] and Clasen et al. [40,62] has actually focused on complex liquids and the effects that confinement of the microstructure has on the effective bulk rheological response. These investigations captured the response of systems containing emulsion droplets, microgels or wax particles with characteristic length scales of 10 - 50 µm.

The aim of this paper is to demonstrate how the measuring range of the flexure-based microgap rheometer (FMR) [40] can be expanded to investigate the shear rheology in the largely unexplored range corresponding to sample gaps from the range of ~10 µm down to ~ 200 nm. The paper is structured as follows. First we introduce the new gap control mechanism for the FMR that allows systematic control of the gap below the previous lower limit of 1 µm and we perform an analysis on the source of error-limiting parallelism of the shearing surfaces. In the second part we demonstrate with PDMS melts of different viscosities that the enhanced FMR is capable of reaching shear rates on the order of 10^4 s^{-1} as a result of the narrow gaps attained. In the third part we demonstrate then that even for this simple PDMS melt, a tribological type of response similar to boundary lubrication is observed at low shear rates. This response originates from the interaction of the shearing surfaces via the entrained airborne dust particles.

Experimental

Test Fluids

The test fluids investigated were trimethylsiloxy terminated poly(dimethylsiloxane) (PDMS) samples (Gelest Inc., Tullytown, PA) with nominal viscosities of 1000 cSt, 5000 cSt and 10000 cSt. The weight average molecular weight M_w has been theoretically calculated from the known relationship to viscosity $\eta = 1.3\times10^{-17} M_w^{3.68}$ Pas [81] and is listed in Table 1. The radii of gyration R_g have been obtained from the molecular weights assuming theta dimensions in the melt and the then appropriate relation $6\langle R_g^2 \rangle / M = 0.422$ Å^{2}mol/g for PDMS at T = 298 K [82] and are also listed in table 1.

The modified FMR

The basic configuration of the flexure-based microgap rheometer (FMR) is described in detail by Clasen et al. [40]. The length of the upper, square shearing plate utilized for the present investigation was m = 4.5 mm and both shearing surfaces were made from polished optical flats (Melles Griot, Rochester, NY) with a surface roughness of λ/20 and coated with a 50 nm layer of TiO_2.

Figure 1 The modified FMR

In order to measure and control submicron gaps between these surfaces, the FMR was equipped with an additional inductive proximity sensor (KAMAN Instrumentation SMU 9200-5U, Colorado Springs, CO) as shown in figure 1. This sensor allows determination of the absolute position of the linear translation stage that is used to position the upper shearing plate and to set the gap, with a resolution of ±1 nm. For the present investigation with PDMS, white-light interferometry (WLI) is used in a closed-loop feedback system with three-point nanopositioning stages to set the parallelism and to determine the absolute gap between the shearing surfaces [40]. This is done at the lower limit of WLI corresponding to a gap of ~1 μm. This absolute value for the gap is subsequently used to calibrate the relative output of the additional proximity sensor. A linear translation stage holds the upper plate assembly and

adjusts the gap between the shearing surfaces with a step resolution of ~ 20 nm. This stage is then used in an open-loop configuration to set absolute gaps in the sub-micrometer range with a resolution of ~ 1 nm, as determined by the proximity sensor.

The parallelism error of the FMR, given as the tilt angle error α of the two shearing surfaces with respect to each other, depends on the gap h and the lateral scale l of the shearing surfaces that is probed with the white-light interferometry. The parallelism of the shearing surfaces also determines the lower bound for setting gaps with the FMR in the submicron range. Because the final adjustment of parallelism of the shearing surfaces is performed at the lower limit of the white-light interferometry system with a gap on the order of $h \approx 1$ μm, this parallelism error is propagated forward when imposing smaller gaps. The absolute distance $h(x)$ between the two surfaces at any point x along the length l can be determined from two discrete wavelengths λ_m, λ_{m+k} of the interference fringes that emerge from an optical probe passed through the sample at this point [40]

$$h = \frac{k}{2n_f}\frac{\lambda_m \lambda_{m+k}}{\lambda_m - \lambda_{m+k}},\ k = 1, 2\ldots,$$

where n_f is the refractive index of the medium within the gap. The parallelism error of the FMR is then caused by the uncertainty of the gap, δh, that is related to the accuracy $\delta\lambda$ with which the white light interferometrical setup can determine the wavelength of an interference fringe. This uncertainty equates to $\delta h = h(\lambda_m + \delta\lambda, \lambda_{m+k} + \delta\lambda) - h(\lambda_m, \lambda_{m+k})$ when determining the gap h from two interference fringes of wave lengths λ_m and λ_{m+k}. At the lowest gap (h ~ 1 μm) for which two fringes are still clearly visible (~ λ_m = 600 nm, λ_{m+k} =460 nm) and with an experimentally determined accuracy $\delta\lambda = \pm 0.085$ nm, this gives δh = 0.3 nm. The uncertainty of the gap δh along the length l gives the tilt angle error $\alpha = \delta h/l$ between the shearing surfaces, which calculates to $\alpha = \delta h/l = 3\times10^{-8}$ (where in the current setup l = 2.85 mm is determined by the diameter of the beam of white light that actually enters the spectrometer). The angular misalignment α persists even when closing the gap h to sub-micrometer separations, and is no longer negligible when αm (where m is the actual length of the shearing surface) becomes comparable to the desired gap h. For the current investigations we therefore limit the gap to h > 100 nm, which relates to $h/(\alpha m) > 1.2\times10^{3}$.

Bulk rheological and high shear characterization of the test fluids

The flow curves for the PDMS samples as well as the measured first normal stress differences $N_1(\dot{\gamma})$ as a function of the shear rate $\dot{\gamma}$ were determined using an AR 2000 rotational rheometer (TA Instruments, Newcastle, DE) with a cone and plate fixture (Ø = 4 cm, 1° cone angle). The results of these bulk rheological measurements are presented in Figure 2.

Figure 2 bulk plus high shear data normal force

In addition, the high shear response of the samples was determined utilizing the FMR over a range of (small) gap settings. These results superpose with the bulk rheological measurements and extend to shear rates up to 4×10^4 s^{-1} (the flow curves obtained with the FMR and shown in Figure 2 are truncated to focus just on the hydrodynamic lubrication regime, the full range of data is shown in Figure 3 and discussed in detail below). At these high shear rates, the flow curves for the higher viscosity PDMS samples indicate a shear thinning regime. The onset of this non-Newtonian behaviour is expected for an entangled melt of a linear homopolymer. The observed power laws for the shear stress $\sigma_{21} \sim \dot{\gamma}^1$ and the first normal stress difference $N_1 \sim \dot{\gamma}^2$ follow the expected asymptotic behaviour of an entangled polymer melt in the weakly viscoelastic limit and justify an estimation of an average or effective relaxation time from the relationship

$$\bar{\tau} = \lim_{\dot{\gamma}\to 0} \frac{N_1}{2\sigma_{21}\dot{\gamma}} . \qquad (1)$$

The average relaxation times obtained from this asymptotic result (see Table 1) are in good agreement with the time constant $\tau_{crit} \approx 1/\dot{\gamma}_{crit}$ representing the inverse of the critical shear rate for onset of shear-thinning. These values are obtained from fitting the flow curves in Figure 2 with the empirical Carreau-Yasuda model[83] with the infinite shear viscosity set to $\eta_\infty = 0$:

$$\sigma_{21} = \eta_0 \dot{\gamma}\left[1+\left(\tau_{crit}\dot{\gamma}\right)^b\right]^{\frac{n-1}{b}} . \qquad (2)$$

The fit parameters are given in Table 1. Viscous heating as a source for the observed shear thinning is a concern for high shear rate experiments [29], but this can be ruled out because of the narrow gap. Recalling the definition of the Nahme number $Na = \eta_0 \beta h^2 \dot{\gamma}^2 / kT$ as a dimensionless ratio of the time scales for thermal diffusion to viscous heating, with thermal

sensitivity $\beta = (T/\eta_0)\left|d\eta/dT\right|_{T=T_0}$ [23], it becomes clear that, for the FMR, the Nahme number scales with $Na \propto h^2\dot{\gamma}^2 = V_p{}^2$ where V_p is the velocity of the moving plate. Because the shear experiments at different gaps were always conducted over the same velocity range and in particular to the same maximum velocity $V_{\max}$ = 2 mm/s, the maximum Nahme number can be calculated for PDMS with β = 5.73 at room temperature [84] to be $Na_{max} = 1.9\times10^{-6}$ and is independent of the gap. We can therefore attribute the shear thinning observed experimentally solely to the viscoelastic material response.

Table 1

The Carreau-Yasuda fit to the data also allows an estimation of evolution of the normal stress difference in the bulk sample at high shear rates that exceed the experimentally accessible shear rate range of the AR 2000 rotational rheometer. In particular the expected deviation from the powerlaw $N_1 \sim \dot{\gamma}^2$ can be seen in figure 2 as the critical rate $\dot{\gamma} = 1/\overline{\tau}$ is approached. A simplistic description of the first normal stress difference, sufficient to estimate the onset of the non-rate dependent regime, can be obtained from an upper-convected Maxwell model that incorporates a rate dependence of the material functions, as for example the White-Metzner model [85,86]

$$\boldsymbol{\sigma} + \frac{\eta}{G}\overset{\nabla}{\boldsymbol{\sigma}} = 2\eta\mathbf{D} \qquad (3)$$

where the viscosity is assumed to be a function of the shear rate $\eta = f\left(\sqrt{2\mathbf{D}:\mathbf{D}}\right)$. Here $\mathbf{D}$ represents the rate of deformation tensor $2\mathbf{D} = \nabla\mathbf{v}^T + \nabla\mathbf{v}$, $\boldsymbol{\sigma}$ represents the stress tensor and $\overset{\nabla}{\boldsymbol{\sigma}}$ represents the upper-convected derivative $\overset{\nabla}{\boldsymbol{\sigma}} = \dot{\boldsymbol{\sigma}} - \nabla\mathbf{v}^T\cdot\boldsymbol{\sigma} - \boldsymbol{\sigma}\cdot\nabla\mathbf{v}$ with $\dot{\boldsymbol{\sigma}}$ denoting the substantial time derivative and $\nabla\mathbf{v}^T$ the velocity gradient tensor [87]. Evaluating the first normal stress difference for a simple steady shearing flow gives $N_1 = 2(\eta\dot{\gamma})^2/G$. Inserting the Yasuda-Carreau model for the rate dependent viscosity allows us to describe the rate dependence of N_1 with the model parameters of Table 1:

$$N_1 = 2\eta_0\overline{\tau}\dot{\gamma}^2\left[1+(\tau_{crit}\dot{\gamma})^b\right]^{\frac{2(n-1)}{b}} \qquad (4)$$

The resulting curves are shown in Figure 2 by the broken lines and are in good agreement with the experimental values obtained for N_1 in the initial quadratic flow regime, and allow an estimate of N_1 at the higher shear rates encountered in the FMR.

FMR results at submicron gaps

Figure 3 shows the shear stress measured in the FMR as a function of the shear rate for the three different PDMS samples as the gap is progressively reduced.

Figure 3 FMR results

The results for high shear rates for each gap setting were already presented in Figure 2. However, it is clear from Figure 3 that, at lower shear rates, the PDMS samples show a systematic deviation from the expected simple Newtonian flow behavior when the gap separation is reduced below a critical limit. These deviations can be interpreted in terms of the tribological response of the sample with three characteristic regimes as indicated in figure 3.

At low shear rates, in the so called *'boundary lubrication'* regime, the shear stress is virtually independent of the relative velocity between the shearing surfaces and hence independent of the nominal shear rate $\dot{\gamma} = V_p / h$. This is counterintuitive for the rheologist for whom rate-independent stresses are normally encountered only for idealized yielding processes, but such observations are a regular tribological result of a sliding friction process for which the friction coefficient μ is constant and independent of the velocity difference between the shearing surfaces. What is at a first glance surprising is the observation of a boundary lubrication regime for controlled absolute gaps in the micrometer range. In contrast to a tribological test, the plates of the FMR are not forced into contact by an applied normal load which would lead to a dominant sliding friction response at low rates. This frictional contact arises from rigid asperities that are not on the surfaces but within the liquid itself. Granick and co-workers have previously reported on the effect of airborne dust particles in apparently simple fluids that prevented them from approaching shearing gaps below 3 µm; entrapment of these particles between the surfaces caused damage to their sensitive surface coatings [12]. Also previous FMR investigations for a polybutadiene melt [40] and a polystyrene/styrene oligomer based Boger fluid [62] in a non-dust free environment have shown the onset of sliding friction caused by a

contamination with ambient dust particles at a gap separation of ~ 4 μm. This additional friction contribution can be observed even though we still have a fluid layer of defined and constant thickness in the gap. This is a consequence of the fact that the viscous shear stress response of the thin fluid layer is a function of the applied shear rate, whereas the additional frictional stress caused by the confined particulate phase is independent of the rate. It thus can dominate once the fluid shear stress drops to values significantly below the constant frictional stress. For the present case it can be ruled out that the sliding friction is caused by a confinement of the PDMS itself, as the dimensions of the polymer coils, reported as radii of gyration in Table 1, are of the order of O(10 nm) and therefore at least 2 decades below the gaps for which we can already observe the onset of boundary lubrication in figure 3.

In the '*hydrodynamic lubrication'* regime observed at higher velocities and high shear rates in figure 3 the total measured stress response is dominated by the viscous response of the fluid. In a typical tribological experiment the pressure that arises from hydrodynamic lubrication in this regime forces the shearing surfaces apart against the applied normal load until, at a certain fluid film thickness, the two forces balance. In the FMR, the situation is similar, although the gap is not determined by a force balance between the pressure field in the fluid and the applied normal load, but is directly controlled and set to a constant value throughout the experiment. The stresses that arise from the sheared fluid film are larger than any direct frictional stress between the surfaces. Not surprisingly the hydrodynamic lubrication regimes measured in these simple fluids directly match the bulk flow curves, independent of the gap setting, a feature that has been utilized already in figure 2 in order to obtain the high shear rate part of the flow curve.

The transition regime between the boundary and hydrodynamic lubrication regime at intermediate shear rates is commonly called the *'mixed lubrication'* regime [88]. In tribological experiments this regime is known to be very sensitive to a range of parameters from surface roughness to the internal microstructure of the fluid [89] and therefore it is often most interesting for the investigation of the lubricating properties of a certain surface/liquid combination. In general, the mixed lubrication regime results in a lower coefficient of friction than boundary lubrication and a non-monotonous variation of the shear stress with the shear rate. This is again counterintuitive to the rheologist on a first glance who would demand a monotonous increase of stress with rate for simple shear. However, in tribological terms a transition from a static friction, or 'stick-slip motion', to a sliding friction when increasing the sliding velocity

goes along with a reduction of the shear stress, thus allowing a non-monotonous variation. Although the FMR does not result in direct contact of the shearing surfaces in the boundary lubrication regime, the frictional forces that are transmitted via the trapped dust particles show a similar drop with increasing shear rate in figure 3.

The curves in figure 3 showing the three distinct lubrication regimes are generally termed 'Stribeck' curves in the tribological literature [39], however, different variables are plotted on the two axes. Conventional tribometers are generally only configured to determine a frictional force response of a sheared sample as a function of an applied velocity under a constant normal load. The results of tribology measurements are therefore commonly reported in terms of quantities that do not require knowledge of the size, shape or separation of the shearing surface. For example the dimensionless sliding friction μ is obtained from the measured shear force F_S normalized by the applied normal force F_N.

$$\mu = \frac{F_S}{F_N} = \frac{\sigma_{21}}{\sigma_{11} - \sigma_{22}} \qquad (5)$$

In the boundary lubrication regime $F_S \propto F_N$ and the coefficient of friction is then independent of the applied normal load, by definition. Knowledge of the contact area *A* of the shearing surfaces and the simplicity of the flow field in the FMR allows, in principle, conversion of the friction coefficient into the shear stress and normal stress difference and vice versa, allowing one to translate tribological to rheological terminology. However, the normal force necessary to maintain the gap in the FMR cannot be measured in the current configuration, so the Stribeck curves in figure 3 are given solely in terms of the shear stress σ_{21} and therefore do not superpose in the boundary lubrication regime.

Regular tribometers are also generally not able to determine the gap between the shearing surfaces (although Spikes et al. [90] have proposed an interferometric method to determine a film thickness in rolling friction). They therefore lack the possibility of calculating an absolute shear rate. In tribology, the sliding velocity, associated with the Stribeck curves is therefore normally reported in terms of a dimensionless Sommerfeld number on the x-axis:

$$So = \frac{\eta U}{P}, \qquad (6)$$

where *U* is the linear velocity of the shearing surface, η is the nominal viscosity of the fluid (normally taken to be independent of the shear rate), and *P* is the normal force F_N per unit length of contact *x*. Scaling by the normal force allows superposition of the friction coefficient

for Newtonian liquids in the hydrodynamic lubrication regime, and the introduction of the viscosity into equation (6) allows superposition for Newtonian fluids of different viscosities [91]. Although the gap h between the shearing surfaces of the FMR is known, conversion from shear rate $\dot{\gamma}$ to the Sommerfeld number using $U = \dot{\gamma}h$ is not possible since F_N cannot be determined. The Stribeck curves in figure 3 are therefore given directly as a function of the shear rate $\dot{\gamma}$. This corresponds in rheological terms to normalization of the sliding velocity U by the gap h, hence a superposition of data for different gaps is observed.

While the present version of the FMR is not capable of applying a normal force, it is able to set and maintain a defined sample gap. In this sense the FMR data is complementary to that provided by regular tribometers. In a typical tribometer, even the minimum applied normal load results in such a large compressive normal stress of the samples that the average separation between the two shearing surfaces is reduced to the scale of the surface asperities. By contrast, the gap separation at which the FMR can detect a transition to boundary lubrication is several orders of magnitude larger. This can clearly be seen in figure 3; at low shear rates we are able to detect a transition to constant shear stresses corresponding to boundary lubrication even at gaps of 1-2 µm.
The plateau values of the steady shear stress in the boundary lubrication regime,

$$\bar{\sigma}_p = \lim_{\dot{\gamma}\to 0} \sigma_{21}, \qquad (7)$$

that can be obtained from figure 3 are plotted as a function of the gap separation h in figure 4 for the three PDMS samples. The FMR is capable of resolving these frictional stresses $\bar{\sigma}_p$ over a range of O(10^0 – 10^4 Pa).

Figure 4 stress vs gap

The plateau stresses in figure 4 show two distinct regimes: a fast increase of the stress level when the gap is decreased below a critical gap separation $h_c \sim 4$ µm, and subsequently, below a critical separation level of the order $h \sim 2$ µm, an apparent scaling of the stresses with the gap of $\bar{\sigma}_p \sim h^{-3/2}$ (as indicated in figure 4). The initial increase of the plateau stress below h_c is likely to originate from Hertzian contact of the confined particulate structure with the shearing surface. The normal force F_N that originates from the Hertzian contact of an elastic

spherical particle with diameter h_c confined between two flat surfaces separated by a gap h scales as [92]

$$F_N \sim (1-\varepsilon)^{\frac{3}{2}}, \qquad (8)$$

where ε is the compressive strain acting on the particle, defined as

$$\varepsilon = \frac{h}{h_c}. \qquad (9)$$

We can now assume this normal force F_N coupled with the related friction coefficient μ (see equation (5)) as the source for the measured shear force F_S in the boundary lubrication regime observed at low velocities. We obtain then by inserting equation (8) into (5) for the initial plateau stress $\bar{\sigma}_p \sim \mu(1-\varepsilon)^{3/2}$.

However, Hertzian contact forces can only be assumed for small compressive deformations $(1-\varepsilon) \ll 1$. At larger compressions in gaps below $h \sim 2$ μm, assuming a single constant Mooney-Rivlin constitutive model for the compressed elastic particulate phase[87], a more appropriate relation of the normal force to the compressive strain would be

$$F_N \sim \left((1-q)+\frac{q}{\varepsilon}\right)\left(\frac{1}{\varepsilon}-\varepsilon^2\right). \qquad (10)$$

Combining the two regimes into a single expression by inserting equation (8) and (10) into (5), we obtain

$$\bar{\sigma}_p \sim \mu\left((1-q)+\frac{q}{\varepsilon}\right)\left(\frac{1}{\varepsilon}-\varepsilon^2\right)(1-\varepsilon)^{\frac{3}{2}}. \qquad (11)$$

Fits of this expression to the experimental data are shown in figure 4 as solid lines (where the parameter q of the Mooney constitutive equation was taken to be $q = 0.1$ as suggested by Bird *et al.* [87]). The observed apparent scaling of $\bar{\sigma}_p \sim h^{-3/2}$ indicated in figure 4 arises from the transition of the force scaling of the Mooney solid in equation (10) or (11) from $\sim\varepsilon^{-1}$ to $\sim\varepsilon^{-2}$ at a compression level of order of $\varepsilon \sim q$.

Another important observation in figure 4 is that the boundary lubrication stress level $\bar{\sigma}_p$ is not directly related to the viscosity of the samples. In the hydrodynamic lubrication regime the measured stress response of the samples is directly related to the viscosity (see flowcurves in figure 2), However, it can be seen from figure 4 that the 5000cSt sample shows somewhat

lower stress values $\bar{\sigma}_p$ then the 1000cSt or 10000cSt sample at comparable gaps. Again this supports the hypothesis that stress conditions in the boundary lubrication regime are controlled by contact stresses of the confined particulate structure inside the fluid rather than bulk material properties of the fluid such as the shear viscosity. The normal force F_N expressed in either equation (8) or (10) depends on the elastic modulus of the confined particles. Furthermore, the measured shear force F_S that is caused by the confined particulate structure (and therefore also the reported plateau stresses $\bar{\sigma}_p$) depends on the actual contact area between the asperities in the fluid and the shearing surfaces and it therefore depends on the volume fraction of the particulate structure. Although it was not possible to directly visualize the particulate contamination of the three samples (we assume that it consists of airborne dust as suggested by Granick et al. [12]), it is apparent from figure 4 that the type and number density of confined particles in the 5000cSt sample fluid causes less friction then the other two samples at the same gap separation.

Conclusion

The enhanced version of the FMR allows measurement of the viscometric response of viscoelastic fluids over a wide range of controlled separation distances spanning from a minimum of approximately 0.1 µm up to a maximum of 200 µm (see Clasen *et al.* [40]). It has been proven difficult in the past to probe this range with either conventional rheometrical methods or tribological techniques. Even for apparently simple fluids we are able to observe a quasi tribological response at low shear rates; corresponding to boundary lubrication with a constant and rate independent sliding frictional stress. In contrast to conventional rheometry or tribometry, this friction does not originate from direct contact of asperities on the shearing surfaces themselves, but is transmitted between the surfaces by the confined particulate structure in the fluid. The boundary lubrication stress thus does not depend on the bulk fluid viscosity, but rather on the specific characteristics of the confined particulate phase. This has been demonstrated for three PDMS melts of differing viscosity levels, for which the stress level measured in the boundary lubrication regime did not scale with the viscosity of the test fluid. FMR data at constant gaps are thus complementary to general tribological investigations under constant applied normal loads. In the boundary lubrication regime the FMR is capable of resolving frictional stresses $\bar{\sigma}_p$ over a range of O(10 – 10^4 Pa). By

contrast, tribological experiments typically operate at a much higher level of confinement (and resulting frictional stress) than the FMR.

With increasing shear rate, the viscous stresses developed in the bulk fluid film eventually overcome the sliding frictional stress associated with the boundary lubrication regime and the FMR measures the bulk flow curves of the PDMS melts. As expected these are independent of the gap level down to the minimum separation distances of ~ 150 nm. Because of the very small separation between the shearing surfaces the FMR is capable of achieving high shear rates up to 10^4 s^{-1} without concern of viscous heating artifacts, even if the liquid being probed is extremely viscous.

References

[1] Crocker JC, Valentine MT, Weeks ER, Gisler T, Kaplan PD, Yodh AG and Weitz DA: Two-point microrheology of inhomogeneous soft materials, Physical Review Letters 85 (2000) 888-891.

[2] Mason TG, Ganesan K, vanZanten JH, Wirtz D and Kuo SC: Particle tracking microrheology of complex fluids, Physical Review Letters 79 (1997) 3282-3285.

[3] Gittes F, Schnurr B, Olmsted PD, MacKintosh FC and Schmidt CF: Microscopic viscoelasticity: Shear moduli of soft materials determined from thermal fluctuations, Physical Review Letters 79 (1997) 3286-3289.

[4] Levine AJ and Lubensky TC: One- and two-particle microrheology, Physical Review Letters 85 (2000) 1774-1777.

[5] Bishop AI, Nieminen TA, Heckenberg NR and Rubinsztein-Dunlop H: Optical microrheology using rotating laser-trapped particles, Physical Review Letters 92 (2004) 4.

[6] Pine DJ, Weitz DA, Chaikin PM and Herbolzheimer E: Diffusing-wave spectroscopy, Physical Review Letters 60 (1988) 1134-1137.

[7] Popescu G, Dogariu A and Rajagopalan R: Spatially resolved microrheology using localized coherence volumes, Physical Review E 65 (2002) art. no. 041504.

[8] Boskovic S, Chon JWM, Mulvaney P and Sader JE: Rheological measurements using microcantilevers, Journal of Rheology 46 (2002) 891-899.

[9] Montfort JP, Tonck A, Loubet JL and Georges JM: Microrheology of high-polymer solutions, Journal of Polymer Science, Part B: Polymer Physics 29 (1991) 677-682.

[10] Waigh TA: Microrheology of complex fluids, Reports on Progress in Physics 68 (2005) 685-742.

[11] McKenna GB: Commentary on rheology of polymers in narrow gaps, European Physical Journal E 19 (2006) 101-108.

[12] Dhinojwala A and Granick S: Micron-gap rheo-optics with parallel plates, Journal of Chemical Physics 107 (1997) 8664-8667.

[13] Moon D, Bur AJ and Migler KB: Multi-sample micro-slit rheometry, Journal of Rheology 52 (2008) 1131-1142.

[14] Aramphongphun C and Castro JM: Microfluidics and rheology of dilute carbon black suspensions for in-mould coating (imc) applications, Modelling and Simulation in Materials Science and Engineering 15 (2007) 157-170.

[15] Son Y: Development of a pressure-driven micro-rheometer, Polymer Testing 27 (2008) 243-247.

[16] Xie Z, Zou Q and Yao DG: Design and verification of the pressure-driven radial flow microrheometer, Tribology Transactions 51 (2008) 396-402.

[17] Han Z, Tang X and Zheng B: A pdms viscometer for microliter newtonian fluid, Journal of Micromechanics and Microengineering 17 (2007) 1828-1834.

[18] Srivastava N, Davenport RD and Burns MA: Nanoliter viscometer for analyzing blood plasma and other liquid samples, Analytical Chemistry 77 (2005) 383-392.

[19] Guillot P, Panizza P, Salmon JB, Joanicot M, Colin A, Bruneau CH and Colin T: Viscosimeter on a microfluidic chip, Langmuir 22 (2006) 6438-6445.

[20] Nguyen NT, Yap YF and Sumargo A: Microfluidic rheometer based on hydrodynamic focusing, Measurement Science & Technology 19 (2008) 9.

[21] Degre G, Joseph P, Tabeling P, Lerouge S, Cloitre M and Ajdari A: Rheology of complex fluids by particle image velocimetry in microchannels, Applied Physics Letters 89 (2006) 3.

[22] Chevalier J and Ayela F: Microfluidic on chip viscometers, Review of Scientific Instruments 79 (2008) 3.

[23] Pipe CJ, Majmudar TS and McKinley GH: High shear rate viscometry, Rheologica Acta 47 (2008) 621-642.

[24] Duda JL, Klaus EE and Lin SC: Capillary viscometry study of non-newtonian fluids - influence of viscous heating, Industrial & Engineering Chemistry Research 27 (1988) 352-361.

[25] Erickson D, Lu FZ, Li DQ, White T and Gao J: An experimental investigation into the dimension-sensitive viscosity of polymer containing lubricant oils in microchannels, Experimental Thermal and Fluid Science 25 (2002) 623-630.

[26] Kang K, Lee LJ and Koelling KW: High shear microfluidics and its application in rheological measurement, Experiments in Fluids 38 (2005) 222-232.

[27] Connelly RW and Greener J: High-shear viscometry with a rotational parallel-disk device, Journal of Rheology 29 (1985) 209-226.

[28] Davies GA and Stokes JR: Thin film and high shear rheology of multiphase complex fluids, Journal of Non-Newtonian Fluid Mechanics 148 (2008) 73-87.

[29] Dontula P, Macosko CW and Scriven LE: Does the viscosity of glycerin fall at high shear rates?, Industrial & Engineering Chemistry Research 38 (1999) 1729-1735.

[30] Kramer J, Uhl JT and Prudhomme RK: Measurement of the viscosity of guar gum solutions to 50,000 1/s using a parallel plate rheometer, Polymer Engineering and Science 27 (1987) 598-602.

[31] Kulicke WM and Porter RS: High shear dependence of the viscosity of polymer fluids, Journal of Rheology 24 (1980) 890-891.

[32] Mriziq KS, Dai HJ, Dadmun MD, Jellison GE and Cochran HD: High-shear-rate optical rheometer, Review of Scientific Instruments 75 (2004) 2171-2176.

[33] Merrill EW: A coaxial cylinder viscometer for the study of fluids under high velocity gradients, J. Coll. Sci. 9 (1954) 7-19.

[34] Barnes HA: Viscosity, The University of Wales Institute of Non-Newtonian Fluid Mechanics, Aberystwyth (2002).

[35] Mhetar V and Archer LA: Slip in entangled polymer solutions, Macromolecules 31 (1998) 6639-6649.

[36] Barnes HA: A review of the slip (wall depletion) of polymer-solutions, emulsions and particle suspensions in viscometers - its cause, character, and cure, Journal of Non-Newtonian Fluid Mechanics 56 (1995) 221-251.

[37] Reimers MJ and Dealy JM: Sliding plate rheometer studies of concentrated polystyrene solutions: Nonlinear viscoelasticity and wall slip of two high molecular weight polymers in tricresyl phosphate, Journal of Rheology 42 (1998) 527-548.

[38] Migler KB, Hervet H and Leger L: Slip transition of a polymer melt under shear-stress, Physical Review Letters 70 (1993) 287-290.

[39] Granick S, Zhu YX and Lee H: Slippery questions about complex fluids flowing past solids, Nature Materials 2 (2003) 221-227.

[40] Clasen C, Gearing BP and McKinley GH: The flexure-based microgap rheometer (fmr), Journal of Rheology 50 (2006) 883-905.

[41] Ho BP and Leal LG: Creeping motion of liquid drops through a circular tube of comparable diameter, Journal of Fluid Mechanics 71 (1975) 361-375.

[42] Coutanceau M and Thizon P: Wall effect on the bubble behavior in highly viscous liquids, Journal of Fluid Mechanics 107 (1981) 339-373.

[43] Olbricht WL and Kung DM: The deformation and breakup of liquid drops in low reynolds-number flow through a capillary, Physics of Fluids a-Fluid Dynamics 4 (1992) 1347-1354.

[44] Graham DR and Higdon JJL: Oscillatory flow of droplets in capillary tubes. Part 1. Straight tubes, Journal of Fluid Mechanics 425 (2000) 31-53.

[45] Graham DR and Higdon JJL: Oscillatory flow of droplets in capillary tubes. Part 2. Constricted tubes, Journal of Fluid Mechanics 425 (2000) 55-77.

[46] Mietus WGP, Matar OK, Lawrence CJ and Briscoe BJ: Droplet deformation in confined shear and extensional flow, Chemical Engineering Science 57 (2002) 1217-1230.

[47] Son Y, Martys NS, Hagedorn JG and Migler KB: Suppression of capillary instability of a polymeric thread via parallel plate confinement, Macromolecules 36 (2003) 5825-5833.

[48] Vananroye A, Van Puyvelde P and Moldenaers P: Effect of confinement on droplet breakup in sheared emulsions, Langmuir 22 (2006) 3972-3974.

[49] Migler KB: String formation in sheared polymer blends: Coalescence, breakup, and finite size effects, Physical Review Letters 86 (2001) 1023-1026.

[50] Pathak JA and Migler KB: Droplet-string deformation and stability during microconfined shear flow, Langmuir 19 (2003) 8667-8674.

[51] Hagedorn JG, Martys NS and Douglas JF: Breakup of a fluid thread in a confined geometry: Droplet-plug transition, perturbation sensitivity, and kinetic stabilization with confinement, Physical Review E 69 (2004)

[52] van Roij R, Dijkstra M and Evans R: Interfaces, wetting, and capillary nematization of a hard-rod fluid: Theory for the zwanzig model, Journal of Chemical Physics 113 (2000) 7689-7701.

[53] Dijkstra M: Capillary freezing or complete wetting of hard spheres in a planar hard slit?, Physical Review Letters 93 (2004)

[54] van Blaaderen A, Ruel R and Wiltzius P: Template-directed colloidal crystallization, Nature 385 (1997) 321-324.

[55] Meinhart CD and Zhang HS: The flow structure inside a microfabricated inkjet printhead, Journal of Microelectromechanical Systems 9 (2000) 67-75.

[56] Solomon MJ and Lu Q: Rheology and dynamics of particles in viscoelastic media, Current Opinion in Colloid & Interface Science 6 (2001) 430-437.

[57] Weitz DA and Pine DJ: Diffusing wave spectroscopy in Dynamic light scattering, W Brown, Oxford University Press, Oxford (1992)

[58] Raghu A and Ananthamurthy S: Construction of an optical tweezer for nanometer scale rheology, Pramana-Journal of Physics 65 (2005) 699-705.

[59] Meiners JC and Quake SR: Femto-newton force spectroscopy of single extended DNA molecules, Physical Review Letters 84 (2000) 5014-5017.

[60] Bausch AR, Ziemann F, Boulbitch AA, Jacobson K and Sackmann E: Local measurements of viscoelastic parameters of adherent cell surfaces by magnetic bead microrheometry, Biophysical Journal 75 (1998) 2038-2049.

[61] Gosse C and Croquette V: Magnetic tweezers: Micromanipulation and force measurement at the molecular level, Biophysical Journal 82 (2002) 3314-3329.

[62] Clasen C and McKinley GH: Gap-dependent microrheometry of complex liquids, Journal of Non-Newtonian Fluid Mechanics 124 (2004) 1-10.

[63] MacKintosh FC and Schmidt CF: Microrheology, Current Opinion in Colloid & Interface Science 4 (1999) 300-307.

[64] Gardel ML, Valentine MT and Weitz DA: Microrheology in Microscale diagnostic techniques, K Breuer, Springer, Berlin (2005) 1-50.

[65] Choi J and Kato T: Static and dynamic behavior of liquid nano-meniscus bridge, Tribology Transactions 44 (2001) 19-26.

[66] O'Connell PA and McKenna GB: Novel nanobubble inflation method for determining the viscoelastic properties of ultrathin polymer films, Review of Scientific Instruments 78 (2007) 12.

[67] Cross GLW, Connell BSO, Pethica JB, Rowland H and King WP: Variable temperature thin film indentation with a flat punch, Review of Scientific Instruments 79 (2008) 13.

[68] Israelachvili JN, McGuiggan PM and Homola AM: Dynamic properties of molecularly thin liquid-films, Science 240 (1988) 189-191.

[69] Giasson S, Israelachvili J and Yoshizawa H: Thin film morphology and tribology study of mayonnaise, Journal of Food Science 62 (1997) 640-652.

[70] Mukhopadhyay A and Granick S: Micro- and nanorheology, Current Opinion in Colloid & Interface Science 6 (2001) 423-429.

[71] Hu Y-Z and Granick S: Microscopic study of thin film lubrication and its contributions to macroscopic tribology, Tribology Letters 5 (1998) 81-88.

[72] Soga I, Dhinojwala A and Granick S: Optorheological studies of sheared confined fluids with mesoscopic thickness, Langmuir 14 (1998) 1156-1161.

[73] Fritz G, Pechhold W, Willenbacher N and Wagner NJ: Characterizing complex fluids with high frequency rheology using torsional resonators at multiple frequencies, Journal of Rheology 47 (2003) 303-319.

[74] Crassous JJ, Regisser R, Ballauff M and Willenbacher N: Characterization of the viscoelastic behavior of complex fluids using the piezoelastic axial vibrator, Journal of Rheology 49 (2005) 851-863.

[75] Cagnon M and Durand G: Mechanical shear of layers in smectic-a and smectic-b liquid-crystal, Physical Review Letters 45 (1980) 1418-1421.

[76] Collin D and Martinoty P: Dynamic macroscopic heterogeneities in a flexible linear polymer melt, Physica a-Statistical Mechanics and Its Applications 320 (2003) 235-248.

[77] Meeten GH: Flow of soft solids squeezed between planar and spherical surfaces, Rheologica Acta 44 (2005) 563-572.

[78] Henson DJ and Mackay ME: Effect of gap on the viscosity of monodisperse polystyrene melts - slip effects, Journal of Rheology 39 (1995) 359-373.

[79] Macosko C: Rheology: Principles, measurements, and applications, VCH Publishers, New York (1994).

[80] Davies GA and Stokes JR: On the gap error in parallel plate rheometry that arises from the presence of air when zeroing the gap, Journal of Rheology 49 (2005) 919-922.

[81] Dvornic PR: Some recent advances in the silicone containing polymers in DP Uskokovic, Transtec Publications Ltd, (1996), 131-138.

[82] Fetters LJ, Lohse DJ, Richter D, Witten TA and Zirkel A: Connection between polymer molecular-weight, density, chain dimensions, and melt viscoelastic properties, Macromolecules 27 (1994) 4639-4647.

[83] Yasuda K, Armstrong RC and Cohen RE: Shear-flow properties of concentrated-solutions of linear and star branched polystyrenes, Rheologica Acta 20 (1981) 163-178.

[84] Van Hemelrijck E: Thesis, Katholieke Universiteit Leuven (2005).

[85] White JL and Metzner AB: Development of constitutive equations for polymeric melts and solutions, Journal of Applied Polymer Science 7 (1963) 1869-1891.

[86] Ide Y and White JL: Investigation of failure during elongational flow of polymer melts, Journal of Non-Newtonian Fluid Mechanics 2 (1977) 281-298.

[87] Bird RB, Curtiss CF, Armstrong RC and Hassager O: Dynamics of polymeric liquids. Volume 2: Kinetic theory, Wiley Interscience, New York (1987).

[88] Williams J: Engineering tribology, Cambridge University Press, New York (2005).

[89] Bhushan B: Fundamentals of tribology and bridging the gap between the macro and micro/nanoscales, Kluwer, Boston (2000)

[90] Taylor LJ and Spikes HA: Friction-enhancing properties of zddp antiwear additive: Part ii - influence of zddp reaction films on ehd lubrication, Tribology Transactions 46 (2003) 310-314.

[91] de Vicente J, Stokes JR and Spikes HA: The frictional properties of newtonian fluids in rolling-sliding soft-ehl contact, Tribology Letters 20 (2005) 273-286.

[92] Johnson KL: Contact mechanics, Cambridge University Press, Cambridge (2001).

Tables

Table 1 Parameters of the poly(dimethylsiloxane) (PDMS) samples studied.

PDMS	η_0	M_w	R_g	$\overline{\tau}$	τ_{crit}	n	b
	[Pas]	[g/mol]	[m]	[s]	[s]		
1000 cSt	1.07	4.0×10^{4}	5.3×10^{-9}	1.8×10^{-5}	2×10^{-5}	0.60	0.94
5000 cSt	5.6	6.2×10^{4}	6.6×10^{-9}	2.1×10^{-4}	2×10^{-4}	0.585	1
10000cSt	10.25	7.3×10^{4}	7.1×10^{-9}	3.9×10^{-4}	4×10^{-4}	0.56	0.93

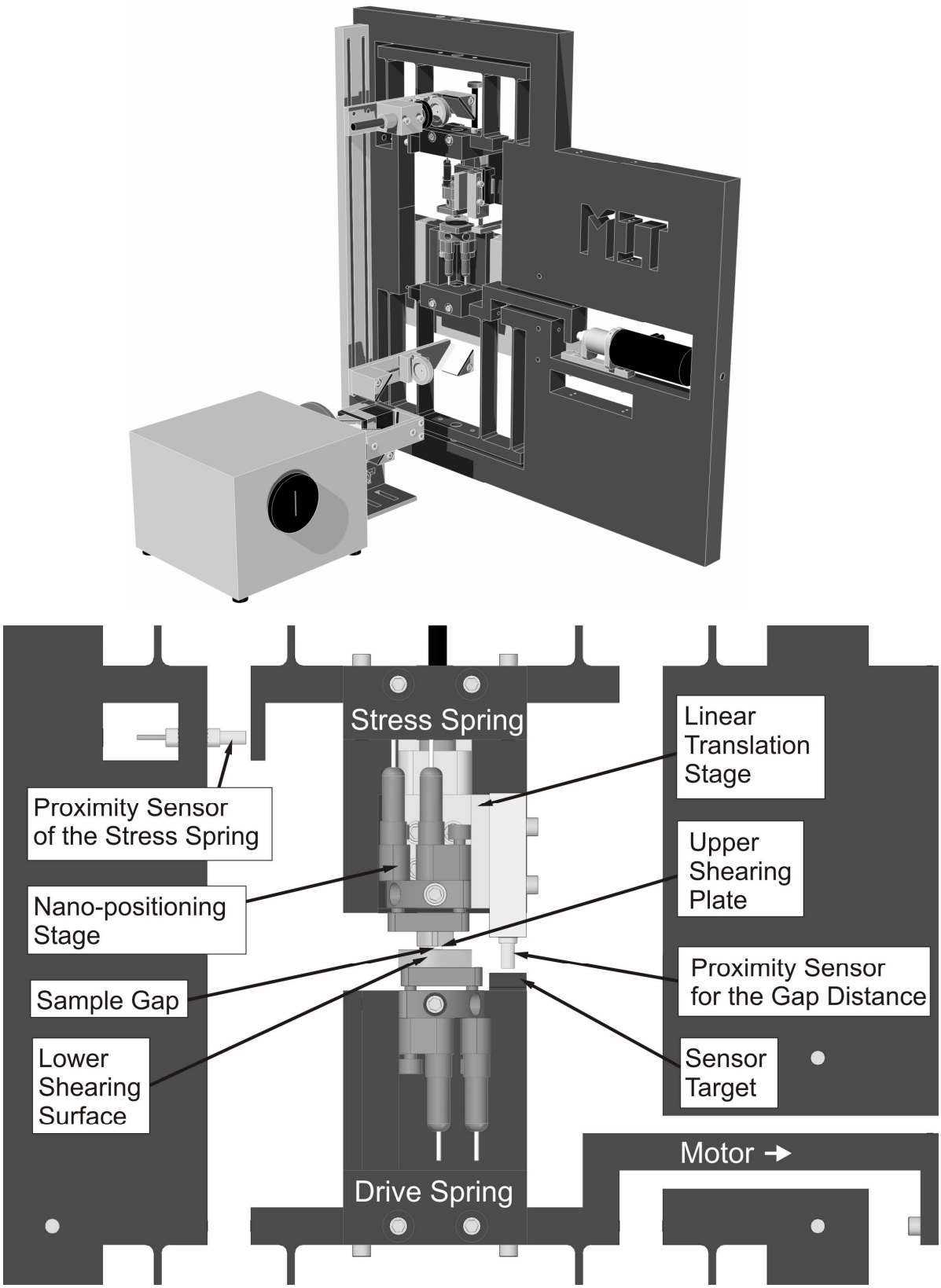

Figure 1 The modified FMR. The additional proximity sensor allows determination of relative sample gap separations between the upper and lower shearing surface even below the resolution of the white light interferometry and extends the accessible gap range to 1 µm > h > 135 nm.

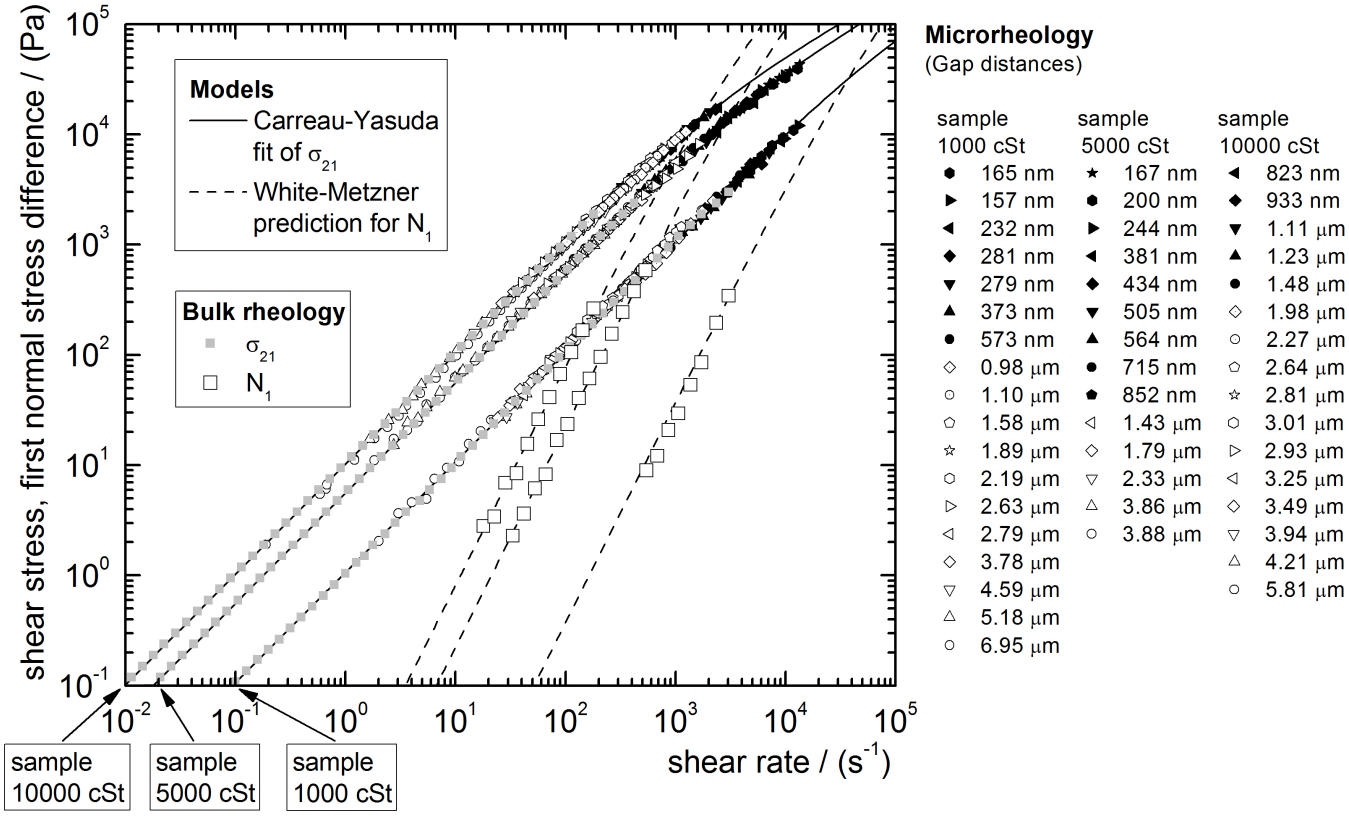

Figure 2 Shear stress and first normal stress difference as function of imposed shear rate. Filled grey squares (σ_{21}) and open squares (N_1) are determined for bulk samples with a cone-and-plate fixture (AR 2000, TA Instruments, Newcastle, DE). All other open and closed symbols represent the shear stress of the hydrodynamic lubrication regime of the microgap rheometer measurements of Figure 3 at different gaps (the gaps reported for open symbols are absolute gaps determined directly with white light interferometry, for closed symbols the gaps are determined with the inductive proximity sensor described in the text). Solid lines represent the Carreau-Yasuda model fits of eq. (2). The dashed lines are calculations of N_1 from the White-Metzner model (eq. (4)) with a viscosity function provided via the Carreau-Yasuda parameters of Table 1.

a)

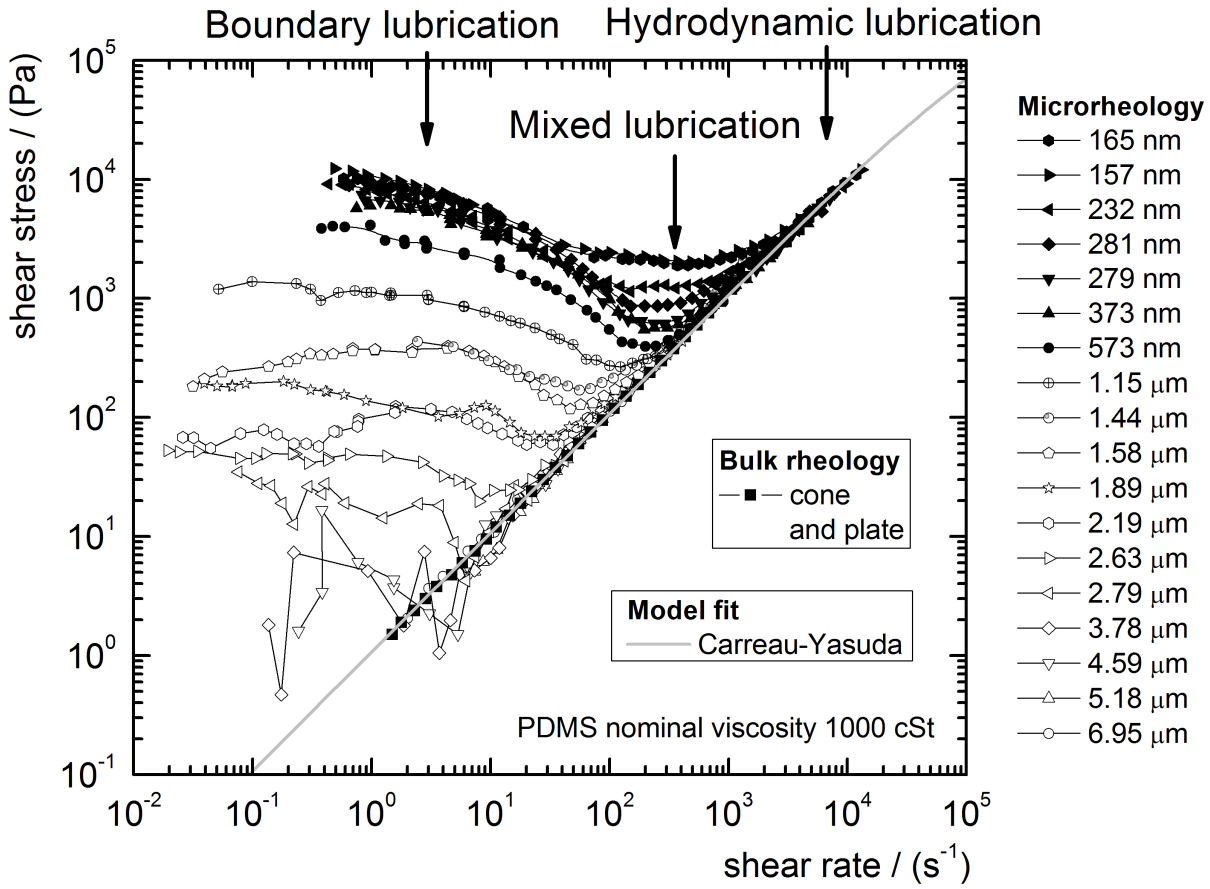
Boundary lubrication
Hydrodynamic lubrication
Mixed lubrication
shear stress / (Pa)
shear rate / (s-1)
Bulk rheology
cone and plate
Model fit
Carreau-Yasuda
PDMS nominal viscosity 1000 cSt
Microrheology
165 nm
157 nm
232 nm
281 nm
279 nm
373 nm
573 nm
1.15 μm
1.44 μm
1.58 μm
1.89 μm
2.19 μm
2.63 μm
2.79 μm
3.78 μm
4.59 μm
5.18 μm
6.95 μm

b)

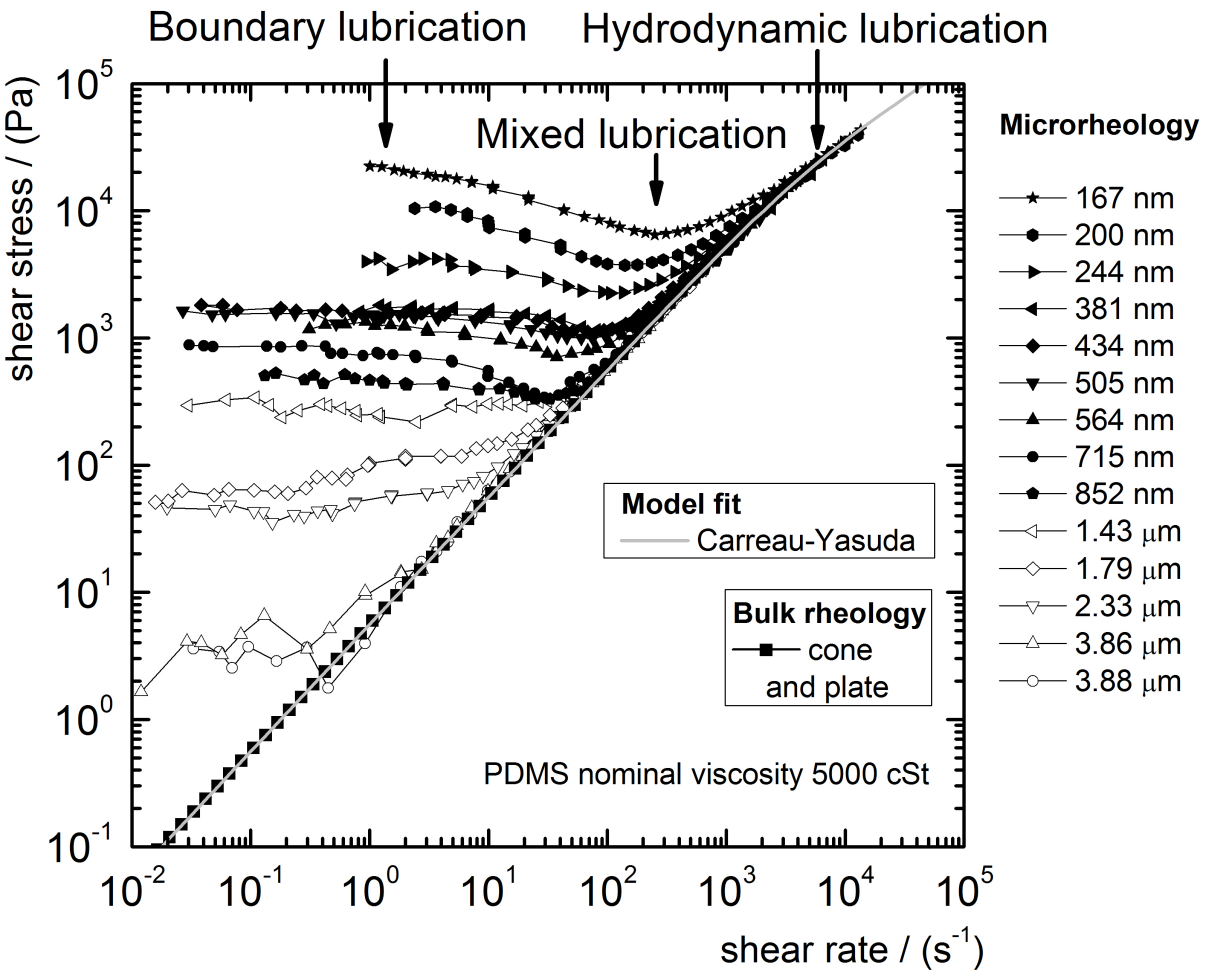
Boundary lubrication
Hydrodynamic lubrication
Mixed lubrication
shear stress / (Pa)
shear rate / (s-1)
Model fit
Carreau-Yasuda
Bulk rheology
cone
and plate
PDMS nominal viscosity 5000 cSt
Microrheology
167 nm
200 nm
244 nm
381 nm
434 nm
505 nm
564 nm
715 nm
852 nm
1.43 μm
1.79 μm
2.33 μm
3.86 μm
3.88 μm

c)

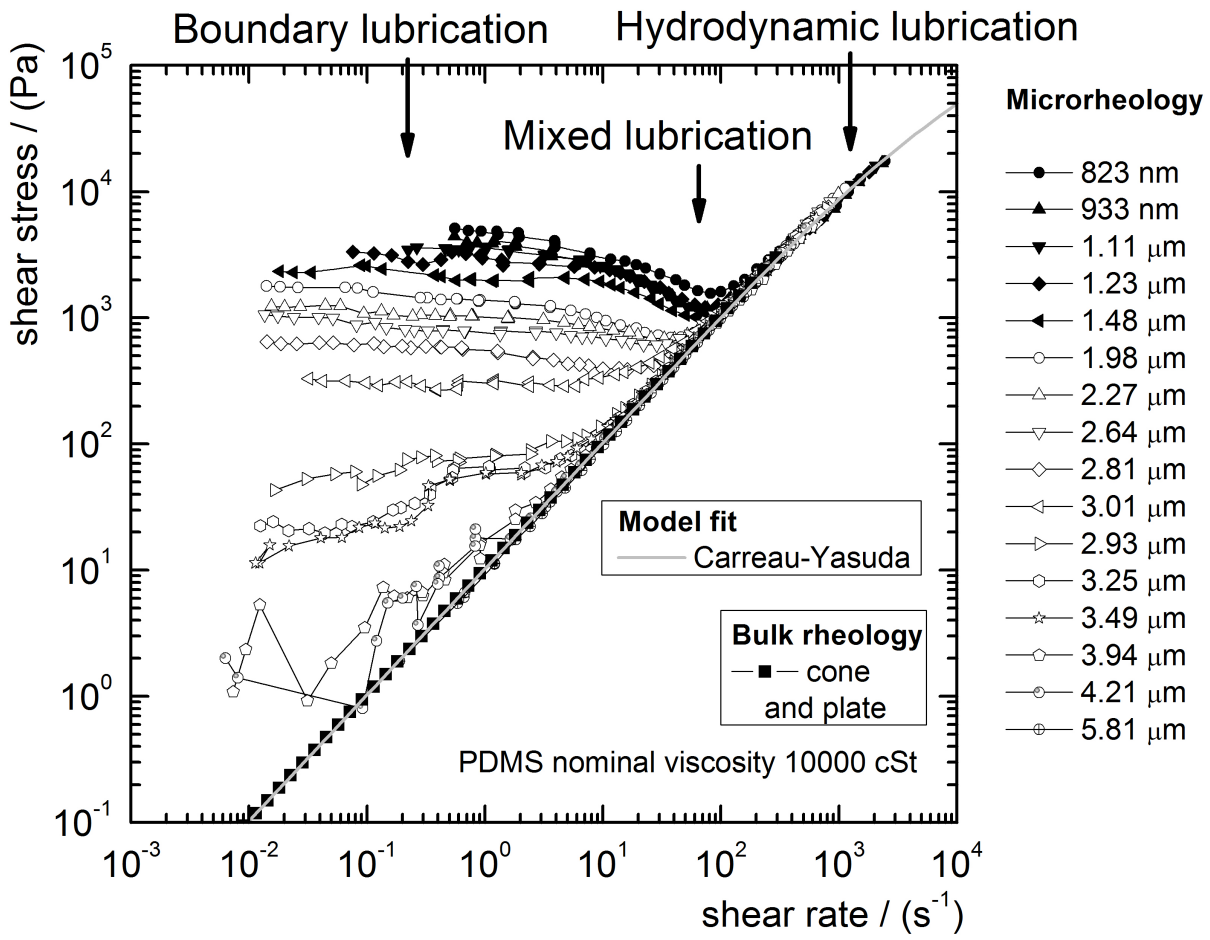

Figure 3 Shear stress as a function of the shear rate, obtained with the microgap rheometer FMR for three different PDMS samples at different, constant separations between the shearing surfaces as indicated in the legend.

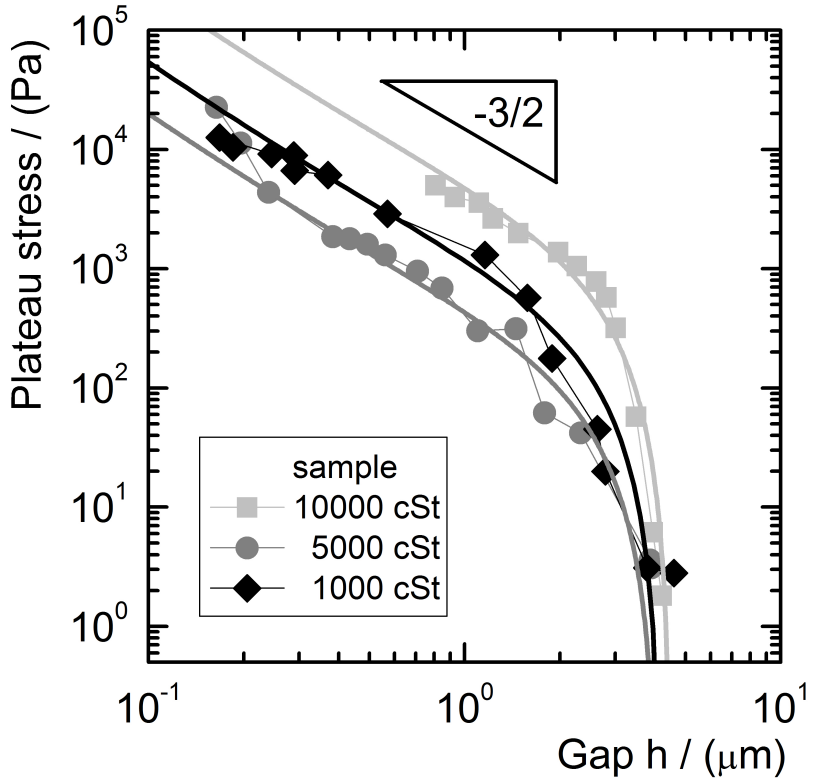

Figure 4 Plateau stress level $\bar{\sigma}_p$ of the boundary lubrication regimes of Figure 3 as a function of the absolute gap *h* for the three investigated PDMS samples. The straight lines represent fits of equation (11) to the experimental data with $q = 0.1$.